

RESEARCH LETTER

10.1002/2015GL065257

Special Section:

First Results from the MAVEN Mission to Mars

Key Points:

- MAVEN observes on almost each periapsis in the nightside ionosphere suprathermal electron depletions
- Observed depletions are populated by 6 eV electrons resulting from absorption by CO₂ and by 3 eV O₂⁺
- The geographical distribution of nightside suprathermal electron depletions depends on altitude

Correspondence to:

M. Steckiewicz,
morgane.steckiewicz@irap.omp.eu

Citation:

Steckiewicz, M., et al. (2015), Altitude dependence of nightside Martian suprathermal electron depletions as revealed by MAVEN observations, *Geophys. Res. Lett.*, 42, doi:10.1002/2015GL065257.

Received 7 JUL 2015

Accepted 18 AUG 2015

©2015. The Authors.

This is an open access article under the terms of the Creative Commons Attribution-NonCommercial-NoDerivs License, which permits use and distribution in any medium, provided the original work is properly cited, the use is non-commercial and no modifications or adaptations are made.

Altitude dependence of nightside Martian suprathermal electron depletions as revealed by MAVEN observations

M. Steckiewicz^{1,2}, C. Mazelle^{1,2}, P. Garnier^{1,2}, N. André^{1,2}, E. Penou^{1,2}, A. Beth^{1,2}, J.-A. Sauvaud^{1,2}, D. Toubanc^{1,2}, D. L. Mitchell³, J. P. McFadden³, J. G. Luhmann³, R. J. Lillis³, J. E. P. Connerney⁴, J. R. Espley⁴, L. Andersson⁵, J. S. Halekas⁶, D. E. Larson³, and B. M. Jakosky⁵
¹Université de Toulouse, UPS-OMP, IRAP, Toulouse, France, ²CNRS, IRAP, Toulouse, France, ³Space Sciences Laboratory, University of California, Berkeley, California, USA, ⁴NASA Goddard Space Flight Center, Greenbelt, Maryland, USA, ⁵Laboratory for Atmospheric and Space Physics, University of Colorado Boulder, Boulder, Colorado, USA, ⁶Department of Physics and Astronomy, University of Iowa, Iowa City, Iowa, USA

Abstract The MAVEN (Mars Atmosphere and Volatile EvolutionN) spacecraft is providing new detailed observations of the Martian ionosphere thanks to its unique orbital coverage and instrument suite. During most periapsis passages on the nightside ionosphere suprathermal electron depletions were detected. A simple criterion was implemented to identify the 1742 depletions observed from 16 November 2014 to 28 February 2015. A statistical analysis reveals that the main ion and electron populations within the depletions are surprisingly constant in time and altitude. Absorption by CO₂ is the main loss process for suprathermal electrons, and electrons that strongly peaked around 6 eV are resulting from this interaction. The observation of depletions appears however highly dependent on altitude. Depletions are mainly located above strong crustal magnetic sources above 170 km, whereas the depletions observed for the first time below 170 km are globally scattered onto the Martian surface with no particular dependence on crustal fields.

1. Introduction

The Mars Atmosphere and Volatile EvolutionN (MAVEN) mission is designed to study the structure, composition, and variability of the upper atmosphere and ionosphere of Mars, its interaction with the Sun/solar wind, and the atmospheric escape [Jakosky et al., 2015]. Its insertion into orbit around Mars occurred on 21 September 2014. The spacecraft since then reached its mapping orbit which is a highly elliptical precessing orbit with a periapsis at 150 km, a period of 4.5 h and an inclination of 75°. This periapsis can also be lowered down to 125 km during deep-dip campaigns such as in mid-February 2015.

The nightside ionosphere of Mars is a poorly investigated area compared to the dayside one. One of the main observational properties of this region is the presence of recurrent structures characterized by significant depletions in electron fluxes and hence called “nightside suprathermal electron depletions” (hereinafter referred to as electron depletions). The first observations of these structures were obtained during the 400 km mapping orbit of Mars Global Surveyor (MGS) by the Electron Reflectometer instrument that detected on Mars’ optical shadow pronounced decreases of the electron count rates up to 3 orders of magnitude at all energies [Mitchell et al., 2001]. The same structures were then detected by the Mars Express (MEX) Electron Spectrometer [Soobiah et al., 2006]. The statistical analysis of their geographical distribution suggested a strong correlation with crustal magnetic field in both hemispheres [Mitchell et al., 2001; Soobiah et al., 2006; Soobiah, 2009]. Lillis and Brain [2013] showed thanks to MGS data fixed at 02:00 A.M. local time that permanent electron depletions are located in regions of strong horizontal crustal fields whereas intermittent depletions are located in weaker horizontal field regions, only existing for low and moderate solar wind pressure. Duru et al. [2011] also reported these structures from measurements obtained down to 275 km altitude by the Mars Advanced Radar for Subsurface and Ionospheric Sounding on board MEX. These last measurements revealed the diversity of electron depletions which were sometimes correlated with ion flow features or ion density depletion regions. Martian electron depletions appeared different from the plasma holes reported at Venus [Brace et al., 1982] since no local time, latitude, or altitude dependencies were detected [Duru et al., 2011]. However, Soobiah [2009] demonstrated that they could not be distinguished from Venus-like electron

holes without the use of in situ magnetic field measurements and plasma density and temperature calculations. To date the origin of electron depletions stays mysterious, and a few processes have been proposed including plasma escape, recombination with ionized components above closed magnetic field lines, or a photochemical process [Duru *et al.*, 2011].

From late November 2014 to late February 2015 the periapsis of MAVEN occurred in the nightside of Mars. This time period therefore appears ideal to study electron depletions observed by MAVEN at low altitudes never reached before together with a unique complete suite of particles and fields instruments not flown on board MGS (no ion spectrometer) and MEX (no magnetometer). In this study we will combine for the first time (1) electron observations from the Solar Wind Electron Analyzer (SWEA) that measures the energy and angular distributions of 5 eV to 5 keV electrons with up to 2 s resolution (D. L. Mitchell *et al.*, The MAVEN Solar Wind Electron Analyzer (SWEA), *Space Science Reviews*, in preparation 2015), (2) ion composition observations from the SupraThermal And Thermal Ion Composition (STATIC) analyzer that measures the velocity distributions and mass composition of suprathermal and thermal ions (J. P. McFadden *et al.*, MAVEN SupraThermal And Thermal Ion Composition (STATIC) Instrument, submitted to *Space Science Reviews*, 2015), (3) magnetic field measurements from the Magnetometer (MAG) with a resolution of 8 pT [Connerney *et al.*, 2015], and (4) observations from the Solar Wind Ion Analyzer (SWIA) that measures the energy spectrum and angular distribution of solar wind and magnetosheath ions with energy from 5 eV to 25 keV [Halekas *et al.*, 2013].

This study will show how MAVEN sampled electron depletions above strong crustal magnetic sources and above places without any significant ones. Thanks to an exhaustive data set of electron depletions we will investigate the ion and electron populations' characteristics inside the electron depletions. We will also examine the altitude dependence of electron depletions and see if the known influence of crustal magnetic anomalies is dependent on altitude.

2. MAVEN Observations of Electron Depletions

2.1. Case Studies

The measurements of SWEA, STATIC, SWIA, and MAG on two particular orbits of MAVEN are presented in Figures 1 and 2. A nightside pass of MAVEN over a strong magnetic anomaly in the northern hemisphere is shown in Figure 1, whereas a similar pass over a quiet magnetic area is shown in Figure 2. During orbit 740 (Figure 1) the spacecraft came from the dayside, passed its periapsis at a local time of 19:15, 125 km above the geographic location (40°N, 74°E), and went out the induced magnetosphere on the nightside. During orbit 669 (Figure 2) it passed its periapsis at a local time of 20:45, 150 km above the geographic location (50°N, 150°E). In both cases we used multiinstrument observations to identify the different boundaries and key regions of the Martian-induced magnetosphere. The bow shock corresponds to the heating of the interplanetary plasma (H^+ and He^{++}) by the interaction between the supersonic solar wind and the Martian obstacle. The so-called magnetic pileup boundary (MPB) corresponds to the boundary where the solar wind proton and the suprathermal magnetosheath electron density decrease suddenly but not the core solar wind electron fluxes nor the solar wind magnetic field that piles up [Acuña *et al.*, 1998; Bertucci *et al.*, 2003; Nagy *et al.*, 2004]. The ionosphere is the region where the atmospheric photoelectrons dominate and the flux of electrons having an energy greater than ~ 30 eV decreases. This decrease can reach 1 order of magnitude for ~ 100 eV electrons [Mitchell *et al.*, 2001].

During orbit 740, SWEA recorded between 06:29 and 06:36 UTC a large electron depletion (delineated by brown dashed vertical lines) characterized by a decrease of the electron energy flux by more than 2 orders of magnitude at almost all energies. There is however a remaining electron population around 6 eV (Figure 1a). STATIC observations revealed a strong peak around 3 eV inside the depletion (Figure 1b) with mostly O_2^+ , whereas the ionosphere was mainly composed of H^+ , He^{++} , O^+ , and O_2^+ (Figure 1c). Note that for O_2^+ 3 eV corresponds to the ram energy resulting from the satellite speed in the case of a thermalized background of ions. Just after the end of the electron depletion, at 06:36 UTC, the mean O_2^+ energy jumps from 3 to 6 eV which is due to a spacecraft potential effect a priori.

During the electron depletions the spacecraft was in the nightside ionosphere below 160 km altitude and passed over a strong magnetic anomaly between 06:29 and 06:33 UTC as indicated by the observed pronounced increase in magnetic field intensity and in agreement with the model of Morschhauser *et al.* [2014]

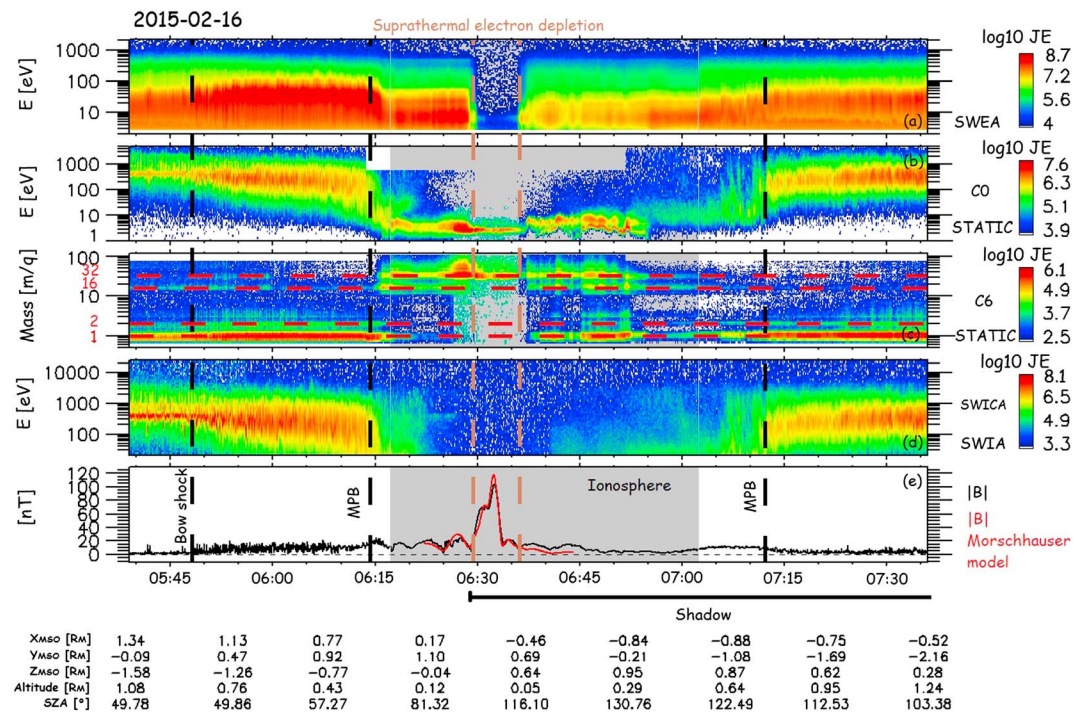


Figure 1. Example of electron depletion in its plasma environment observed above a crustal magnetic field anomaly during orbit 740 on 16 February 2015. (a) SWEA energy-time spectrogram of omnidirectional electron energy flux, (b) STATIC energy-time spectrogram of omnidirectional ion energy flux (C0 mode), (c) STATIC mass-time spectrogram of omnidirectional ion energy flux (C6 mode), (d) SWIA energy-time spectrogram of omnidirectional ion energy flux (SWICA mode), and (e) magnetic field intensity (measured by MAG in black and calculated from the model of Morschhauser *et al.* [2014] in red) versus time. The grey shading highlights the ionosphere. The shadow corresponds to solar zenith angle (SZA) larger than 100°.

(Figure 1d). Electron depletions above magnetic anomalies appear to be a recurrent structure of the nightside ionosphere as reported from MGS and MEX data. Their observations were ascribed to spacecraft crossings of closed magnetic loops whose feet were anchored to crustal magnetic sources on the nightside. Inside those loops the spacecraft was then cut off from solar wind plasma traveling toward the magnetotail and ionospheric plasma coming from the sunlit side [Mitchell *et al.*, 2001]. It was also suggested that electron depletions are not seen on the dayside because when the loops travel on the dayside they are filled with ionospheric photoelectrons. Electron depletions are then the result of a balance between electron loss and creation processes. We can note that between 06:33 and 06:36 UTC the electron depletion is still present, whereas no significant magnetic field can be observed. This phenomenon will be observed in more details in Figure 2.

Figure 2 provides another observation of electron depletions (delineated by brown dashed vertical lines). The depletions are observed between 18:12 and 18:21 UTC below an altitude of 250 km and have similar properties to the depletion described previously. However, within this time interval electron energy flux decreases intermittently and electron depletions are observed alternately with “spikes” [Mitchell *et al.*, 2001]. The main difference with the Figure 1 example is the absence of significant crustal magnetic sources below the spacecraft at the time of the depletion, with very low values of the measured and predicted (by the Morschhauser model, in red in Figure 1e) magnetic fields. The model however predicts a small enhancement of the crustal field of 9 nT at 18:18. This value seems too small to be significant as it is embedded in the ambient magnetic field and coincident with electron spikes. This observation demonstrates that crustal magnetic anomalies cannot be the unique source of electron depletions.

These two case studies have been chosen as representative of a large number of electron depletions observed by MAVEN. The first one above a crustal magnetic anomaly corresponds to the typical case reported previously from MGS and MEX observations. The second one above a quiet magnetic area was occasionally reported from those past observations but is now commonly observed by MAVEN as illustrated by the statistical analysis presented in the next sections.

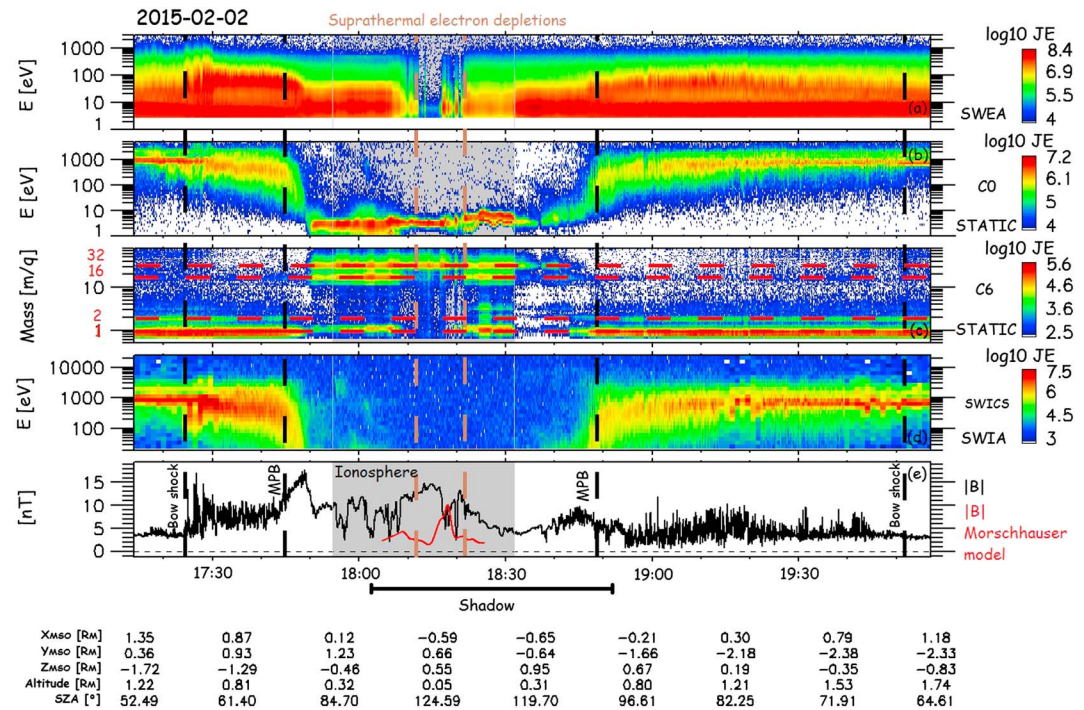


Figure 2. (a–e) Same as Figure 1. Example of electron depletions observed above a quiet magnetic area during orbit 669 on 2 February 2015.

3. Statistical Analysis

3.1. Methodology

A simple but robust criterion was implemented in order to detect electron depletions in MAVEN data. Our criterion is based on electron count rates (CRs) from SWEA observations and is described by equation (1). It relies on three energy channels ($E_1 = 4.26$ eV, $E_2 = 98.93$ eV, and $E_3 = 111.16$ eV) that enable us to distinguish electron depletions from spikes. The sampling time step used is the same as SWEA data: 4 s. Consequently, electron depletions detected last at least 4 s which corresponds to 16 km traveled by the spacecraft. Application of this criterion to data obtained between 16 November 2014 and 28 February 2015 resulted in a data set of 1742 electron depletions identified on 457 orbits among the 494 where data are available. During the 37 others no electron depletion satisfying our criteria was found.

$$\sum_{i=1}^3 \frac{CR(E_i)}{CR(E_i), 1 \text{ h}} < 0.03 \quad (1)$$

3.2. Properties of Electron Depletions

In order to derive the properties of electron depletions we concatenated all time intervals obtained with our criterion. The local time distribution of our data set covers the whole nightside sector, and the solar zenith angle (SZA) distribution varies from 95° to 155° so that some depletions can cross the terminator ($SZA \in [90^\circ, 100^\circ]$). There is therefore no particular local time or SZA dependence detected for the electron depletions considered in this study. However, any dependence with complete local time and solar zenith angle coverage is still undetermined but will be studied with future MAVEN data. Figure 3 provides the measurements of SWEA and STATIC obtained within the depletions. The data gap between 18 and 27 November 2014 corresponds to a safe mode. The different time intervals when low-energy ion populations are not measured by STATIC correspond to a change in instrument mode.

The electron population with energy above 10 eV has disappeared inside the depletions, and the remaining population is strongly peaked around a mean value remarkably constant of 6–7 eV with a full width at half maximum of 2 eV (Figure 3a). The neutral composition of the Martian nightside atmosphere is dominated by CO_2

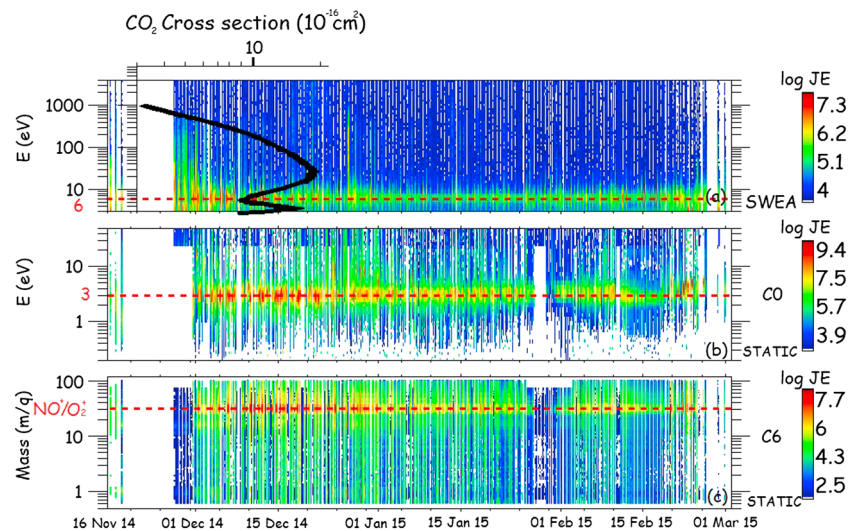


Figure 3. Concatenation of all the time intervals where electron depletions have been detected by our criterion. (a) SWEA energy-time spectrogram of omnidirectional electron energy flux, together with the total electron collision cross section for CO_2 (black line) taken from Itikawa [2002]. (b) STATIC energy-time spectrogram of omnidirectional ion energy flux (C0 mode). (c) STATIC mass-time spectrogram of omnidirectional ions energy flux (C6 mode).

below 200 km [Haider *et al.*, 2013] but also includes O, N_2 , CO, and O_2 . Depending on the model considered the altitude where O becomes dominant is variable [Haider *et al.*, 2013; Krasnopolsky, 2002], but all models describe the same composition. Inspection of the cross section for electron collisions with these five species [Itikawa, 2002; Itikawa and Ichimura, 1990; Itikawa *et al.*, 1986, 1989; Kanik *et al.*, 1993] reveals that only the CO_2 cross section (superimposed on top of the electron time-energy spectrogram in Figure 3a)—due to momentum transfer, excitation, and ionization processes—is in agreement with the inner electron population. It indeed presents a strong dip at 6 eV coincident with the remaining electron population and two strong peaks at 4 and 30 eV. Since a peak in the cross section is related to an electron loss process, electron absorption by the atmospheric CO_2 seems a good candidate to explain the large electron disappearance above 10 eV observed in all depletions as well as the remaining thermal electron population observed between 4 and 12 eV.

The energy of the ion population inside electron depletions (Figure 3b) is also strongly peaked around a mean value of 3 eV with a full width at half maximum of 1 eV on each mode, again suggesting that we observe cold ions with the ram velocity. Looking in detail at the mass-time spectrogram (Figure 3c) enable us to derive the ion composition within electron depletions dominated by O_2^+/NO^+ (Note that STATIC cannot resolve between these species). This observation is consistent with the nightside ionosphere composition calculated by Haider *et al.* [2013] with O_2^+ as the main ion species below 200 km followed by NO^+ and CO_2^+ . In summary the main ion and electron populations of all electron depletions identified in our study appear surprisingly constant independently of the altitude and the period they are observed. We will look into more details to their altitude distribution in the next section.

4. Interpretation

4.1. Altitude Distribution of Electron Depletions

In order to investigate the altitude distribution of all electron depletions we binned our data with constant bins of 2 km altitude. For each bin we first determined the number of electron depletions and then the number of MAVEN's passages contained therein during the time period under study (excluding data gaps during safe mode) in order to remove any orbital bias. The percentage of electron depletions per MAVEN passage is then the ratio of these two numbers, and the result of our statistical binning is provided in Figure 4.

First, the number of electron depletions increases with decreasing altitude. Second, there is a particularly noticeable slope change in our data distribution around 170 km: above 170 km there are 14% of depletions per passage, whereas below 170 km there are 46% of depletions per passage. The percentage even reaches

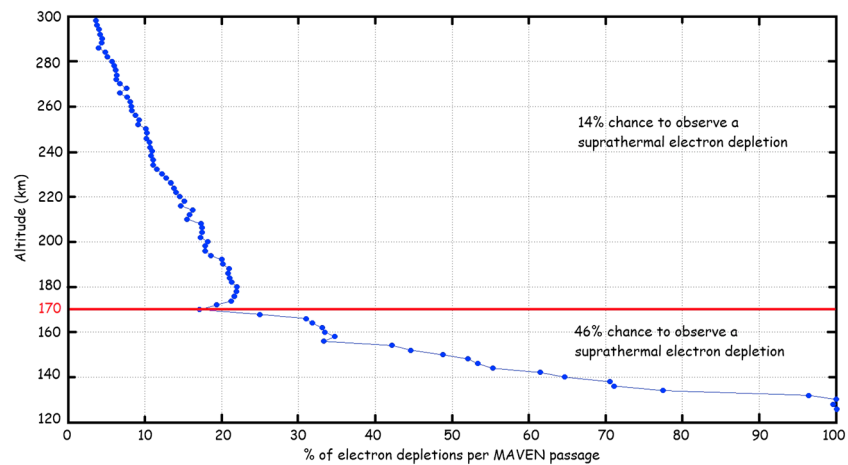


Figure 4. Percentage of electron depletions detected by our criterion per MAVEN passage calculated in bins of 2 km altitude. The horizontal red line highlights the abrupt slope change observed around 170 km.

100% at 125 km during the deep-dip campaign. In order to understand the differences between electron depletion occurrence above and below 170 km we will at first examine the geographic distribution of the electron depletions below this altitude and then above.

4.2. Geographical Distribution of Electron Depletions

We binned the Martian surface with a constant bin size of 5° longitude and 5° latitude and then estimated the percentage of electron depletions per MAVEN passage above each bin. Figure 5 displays the results of our binning for depletions observed below 170 km (Figure 5a) and above 170 km (Figure 5b) with the color-coded percentage of depletions per MAVEN passage projected onto a geographic map of the Martian surface. We superimposed on the resulting map contour lines for the intensity of the magnetic field calculated from the model of *Morschhauser et al.* [2014] at an altitude of 170 km. Only magnetic field intensities greater than 10 nT are indicated for clarity. We note that the number of time steps and of orbits is significant in all cells although weaker at the lowest latitudes (<40°) and altitudes (<150 km).

Figure 5a indicates that the geographic distribution of electron depletions below 170 km is homogeneous above the northern hemisphere between 30°N and 75°N with no significant latitude or longitude dependence. Whereas some of the high percentages bins are located above the two largest magnetic areas located around coordinates (180°E, 45°N) and (10°E, 50°N), many others are not related to them. Therefore, the presence of crustal magnetic sources below the location where electron depletions are observed probably influences their properties, but crustal fields cannot be invoked as the main mechanism to explain their origin in this altitude range. Hence, below a mean altitude of 170 km the predominant process at the origin of electron depletions is electron absorption by atmospheric CO₂.

Contrary to depletions observed below 170 km, Figure 5b indicates a strongly heterogeneous electron depletions distribution above 170 km, mostly observed above the large magnetic areas mentioned previously and very few depletions away from them. This explains why electron depletions previously observed by MEX and MGS were predominantly associated with crustal magnetic fields since their observations were restricted to altitudes above 275 km, which introduced a bias in their interpretation. Hence, the predominant source mechanism at the origin of electron depletions above 170 km seems to be linked with strong crustal magnetic sources. Note however that some depletions do not perfectly fit with the scenario, especially in the regions (230°E, 260°E) and (40°N, 70°N).

5. Conclusions

We have presented new in situ observations of nightside suprathermal electron depletions obtained by MAVEN in the Martian northern hemisphere. These observations are obtained for the first time at low altitudes down to 125 km and nicely extend previous observations of electron depletions by MGS and MEX that

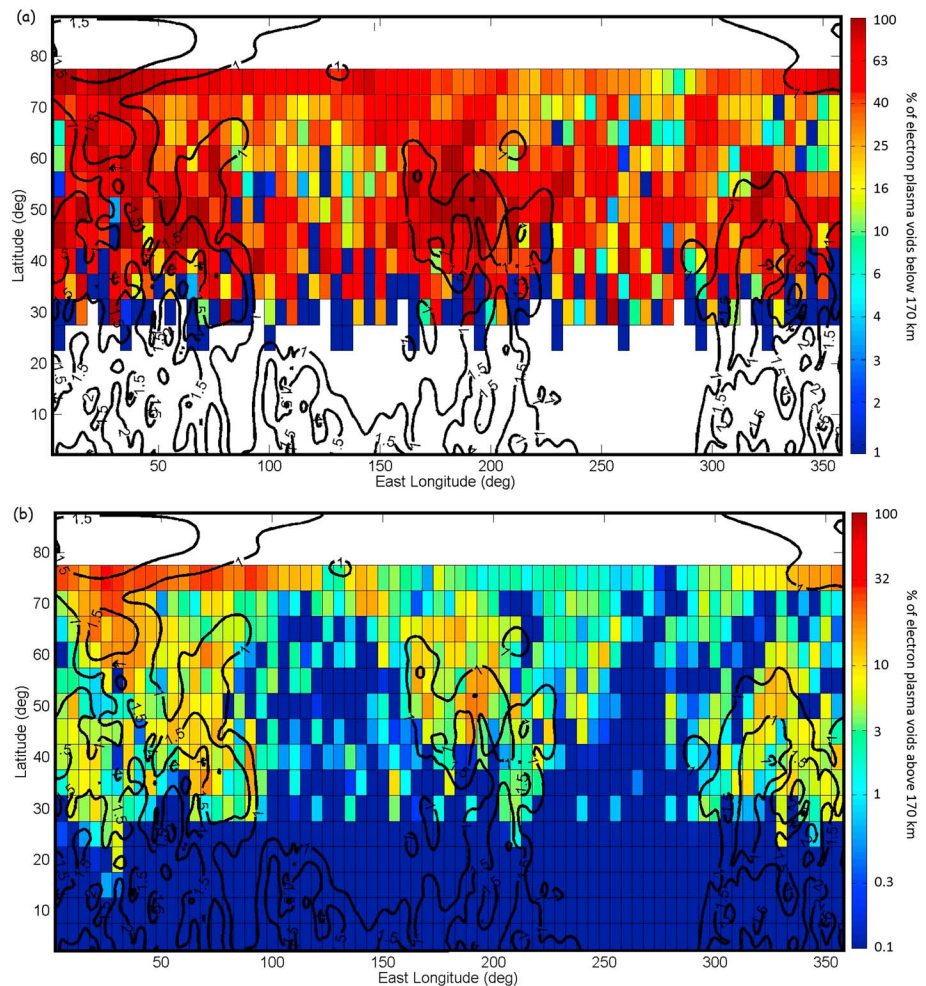


Figure 5. Percentage of electron depletions detected by our criterion per MAVEN passage superimposed on a geographic map of the Martian surface with constant bin size of $5 \times 5^\circ$. The black lines correspond to magnetic field intensity contour lines (in logarithmic scale) calculated from the model of Morschhauser *et al.* [2014] at an altitude of 170 km. Distribution of depletions observed (a) below 170 km and (b) above 170 km.

were restricted to altitudes above 275 km. Taking advantage of the unique suite of particles and field instruments on board MAVEN we showed that the main ion and electron populations inside the electron depletions appear surprisingly constant with time and altitude. Inspection of the cross section for electron collision with the main constituents of the ionosphere suggests that electron absorption by CO_2 is the best candidate to explain the origin of electron depletions. Our statistical analysis however reveals that the presence of electron depletions in the nightside ionosphere is highly dependent on altitude, with the probability of observing an electron depletion above 170 km being 14% compared to 46% below 170 km. Our study indicates that the electron depletions above 170 km—as previously reported by MGS and MEX—are strongly favored by the presence of crustal magnetic fields, whereas electron depletions observed for the first time below 170 km are globally scattered onto the surface of the planet with no particular dependence on crustal fields. Hence, the two main sources of electron depletions highlighted here have different predominance area: low altitude for CO_2 absorption and geographical spots for the crustal magnetic field effect.

MAVEN will soon observe the Martian southern hemisphere where the strongest magnetic crustal sources are located. We naturally plan to extend our analysis in the near future to include these measurements and further test our proposed interpretation about these structures' origin.

Acknowledgments

This work was supported by the French space agency CNES for the part based on observations obtained with the SWEA instrument embarked on MAVEN. The MAVEN project is supported by NASA through the Mars Exploration Program. The authors acknowledge the support of the MAVEN project and particularly all the instrument and science teams for making the MAVEN mission such an outstanding success and providing us with high-quality data. We are also grateful to the CDPP/AMDA team (<http://amda.cdpp.eu>) and Emmanuel Penou for providing support with data analysis tools. MAVEN data are publicly available through the Planetary Data System. The authors thank Yasir Soobiah and an anonymous reviewer for their assistance in evaluating this paper.

The Editor thanks two anonymous reviewers for their assistance in evaluating this paper.

References

- Acuña, M. H., et al. (1998), Magnetic field and plasma observations at Mars: Initial results of the Mars Global Surveyor mission, *Science*, 279(5357), 1676–1680, doi:10.1126/science.279.5357.1676.
- Bertucci, C., et al. (2003), Magnetic field draping enhancement at the Martian magnetic pileup boundary from Mars Global Surveyor observations, *Geophys. Res. Lett.*, 30(2), 1099, doi:10.1029/2002GL015713.
- Brace, L. H., R. F. Theis, H. G. Mayr, S. A. Curtis, and J. G. Luhmann (1982), Holes in the nightside ionosphere of Venus, *J. Geophys. Res.*, 87(A1), 199–211, doi:10.1029/JA087iA01p00199.
- Connerney, J. E. P., J. Espley, P. Lawton, S. Murphy, J. Odom, R. Oliverson, and D. Sheppard (2015), The MAVEN magnetic field investigation, *Space Sci. Rev.*, doi:10.1007/s11214-015-0169-4.
- Duru, F., D. A. Gurnett, D. D. Morgan, J. D. Winningham, R. A. Frahm, and A. F. Nagy (2011), Nightside ionosphere of Mars studied with local electron densities: A general overview and electron density depressions, *J. Geophys. Res.*, 116, A10316, doi:10.1029/2011JA016835.
- Haider, S. A., B. M. Pandya, and G. J. Molina-Cuberos (2013), Nighttime ionosphere caused by meteoroid ablation and solar wind electron-proton-hydrogen impact on Mars: MEX observation and modeling, *J. Geophys. Res. Space Physics*, 118, 6786–6794, doi:10.1002/jgra.50590.
- Halekas, J. S., E. R. Taylor, G. Dalton, G. Johnson, D. W. Curtis, J. P. McFadden, D. L. Mitchell, R. P. Lin, and B. M. Jakosky (2013), The Solar Wind Ion Analyzer for MAVEN, *Space Sci. Rev.*, 1–27, doi:10.1007/s11214-013-0029-z.
- Itikawa, Y. (2002), Cross sections for electron collisions with carbon dioxide, *J. Phys. Chem. Ref. Data*, 31(3), doi:10.1063/1.1481879.
- Itikawa, Y., and A. Ichimura (1990), Cross section for collisions of electrons and photons with atomic oxygen, *J. Phys. Chem. Ref. Data*, 19(3), 637–651.
- Itikawa, Y., M. Hayashi, A. Ichimura, K. Onda, K. Sakimoto, K. Takayanagi, M. Nakamura, H. Nishimura, and T. Takayanagi (1986), Cross sections for collisions of electrons and photons with nitrogen molecules, *J. Phys. Chem. Ref. Data*, 15(3), 985–1010.
- Itikawa, Y., A. Ichimura, K. Onda, K. Sakimoto, T. Takayanagi, Y. Hatano, M. Hayashi, H. Nishimura, and S. Tsurubuchi (1989), Cross sections for collisions of electrons and photons with oxygen molecules, *J. Phys. Chem. Ref. Data*, 18(1), 23–42.
- Jakosky, B. M., et al. (2015), The Mars Atmosphere and Volatile Evolution (MAVEN) mission, *Space Sci. Rev.*, doi:10.1007/s11214-015-0139-x.
- Kanik, I., S. Trajmar, and J. C. Nickel (1993), Total electron scattering and electronic state excitations cross sections for O₂, CO and CH₄, *J. Geophys. Res.*, 98(E4), 7447–7460, doi:10.1029/92JE02811.
- Krasnopolsky, V. A. (2002), Mars' upper atmosphere and ionosphere at low, medium and high solar activities: Implications for evolution of water, *J. Geophys. Res.*, 107(E12), 5128, doi:10.1029/2001JE001809.
- Lillis, R. J., and D. A. Brain (2013), Nightside electron precipitation at Mars: Geographic variability and dependence on solar wind conditions, *J. Geophys. Res. Space Physics*, 118, 3546–3556, doi:10.1002/jgra.50171.
- Mitchell, D. L., R. P. Lin, C. Mazelle, H. Rème, P. A. Cloutier, J. E. P. Connerney, M. H. Acuña, and N. F. Ness (2001), Probing Mars' crustal magnetic field and ionosphere with the MGS Electron Reflectometer, *J. Geophys. Res.*, 106(E10), 23,419–23,427, doi:10.1029/2000JE001435.
- Morschhauser, A., V. Lesur, and M. Grott (2014), A spherical harmonic model of the lithospheric magnetic field of Mars, *J. Geophys. Res. Planets*, 119, 1162–1188, doi:10.1002/2013JE004555.
- Nagy, A. F., et al. (2004), The plasma environment of Mars, *Space Sci. Rev.*, 111(1–2), 33–114, doi:10.1023/B:SPAC.0000032718.47512.92.
- Soobiah, Y. I. J. (2009), The investigation of crustal magnetic field signatures at Mars by the Mars Express ASPERA-3 Electron Spectrometer (ELS), Doctoral thesis, Department of Space and Climate Physics, Mullard Space Science Laboratory, UCL (Univ. College London), London, U. K.
- Soobiah, Y. I. J., et al. (2006), Observations of magnetic anomaly signatures in Mars Express ASPERA-3 ELS data, *Icarus*, 182, 396–405, doi:10.1016/j.icarus.2005.10.034.